Magnetization of ferromagnetic polycrystals subject to an external magnetic field

Huai-Yu Wang[1,*] and Kun Xun[2]
[1]*Department of Physics, Tsinghua University, 100084, Beijing, China*
[2]*Department of Physics, Peking University, 100871, Beijing, China*
(Received 31 July 2006; revised manuscript received 5 November 2006; published 27 December 2006)

We calculate the magnetization of ferromagnetic polycrystals composed of monodomain hard magnetic monocrystals with uniaxial anisotropy under a magnetic field by means of the many-body Green's function method. First, monocrystals are studied. The magnetization rotation of each monocrystal with the field variation is analyzed. When temperature is close to the Curie point, the magnitude of the magnetization changes during the rotation. We find that the abnormal reorientation of the magnetization may cause its component along the field direction to drop. By comparison with the classical model, we suggest an expression connecting the classical anisotropy coefficient K_u to the single-ion anisotropy parameter K_2 in the Heisenberg Hamiltonian and show how K_u varies with temperature. The magnetizing and magnetization reversal processes of the polycrystals are then investigated. It is concluded that the magnetizing curve can be divided into three parts. The discussion includes the susceptibility in the three parts, the remanence, coercivity, and their temperature dependence, the effect of varying anisotropy parameter K_2 and spin quantum number S.

DOI: 10.1103/PhysRevB.74.214425 PACS number(s): 75.40.Cx, 75.30.Cr, 75.60.Jk

I. INTRODUCTION

In a ferromagnetic (FM) polycrystal, the magnetization is the weighted average of all the monocrystals in the sample. When an external field **B** is applied to a magnetic material, the magnetization of each monocrystal will change subject to the field. Here, we only consider the case when each monocrystal has a monodomain structure. In monodomain magnets, the most important change of the magnetization is its rotation or reorientation. Stoner and Wohlfarth investigated the magnetization rotation in such a case via a classical model.[1]

The motivation of this paper is to deal with FM polycrystals by a quantum statistical model based on many-body theory. In this way, the details of the magnetization change should be clearer than in the classical model. With a comparison of our results to those of the classical model, a formula connecting the microscopic anisotropy parameter in the Hamiltonian to the macroscopic one in the classical model can be established.

To study the magnetization rotation, one needs to calculate more than one spatial component of the magnetization as statistical averages of spin operators. The many-body Green's function method (MBGFM) was proven to be a powerful means for calculating the magnetization.[2,3] Although only one component was calculated by the MBGFM before 2000, since then, methods have been developed to calculate all three components of the magnetization in magnetic systems by means of the MBGFM with the random phase approximation (RPA).[4–8]

There have been mainly two kinds of methods used to calculate all three components of the magnetization. One method is to calculate the statistical averages of spin operators simultaneously;[4–7] and the other is to use the frame rotation method (FRM).[8,9]

Fröbrich *et al.*[4,5] first calculated the magnetization of FM films by using three-component Green's functions. Wang *et al.*[6,7] found that under RPA, a general formula for any spin quantum number S could be given for one-, two- and three-dimensional FM systems. This formula was an extension of Callen's method[3] and was applicable to both the case of exchange anisotropy and single-ion anisotropy. Similar to Callen's derivation, the formula of Wang *et al.* proved to be the solution of an ordinary differential equation.[10,11] However, for FM films and for antiferromagnetic (AF) systems, no analytical expression was able to be obtained and one had to resort to numerical calculations. FM films were investigated where the single-ion anisotropy could be in any direction.[12] In another work, the magnetization of sublattices of AF films were studied where external fields were applied along either the longitudinal or transverse direction.[13] It was found that, in the case of the transverse field, the magnetization component along the easy axis did not disappear even above the Néel point. This was because AF exchange should play a role between neighboring spins when they were forced to have a collinear component. This was a unique feature quite different from FM systems. This example showed that the three-component calculation allowed us to understand the magnetic systems more clearly.

In FRM,[8,9] the Cartesian system was first rotated to one in which the magnetization was along the z' axis. In this frame, called primed frame in Ref. 8, the Green's function was simple because the z' component of the spin is conserved. Then after the magnetization was calculated in the primed frame, the components of the magnetization in the original frame were obtained. The merit of this method was that we did not need to construct the three-component Green's functions, and thus saved computation time. Using this method, Jensen *et al.*[14] studied a two-dimensional AF lattice in detail, and verified the feature of AF systems mentioned above.

In this paper, by means of FRM, we study a FM polycrystal composed of monocrystals with uniaxial anisotropy. First, the magnetization of a monocrystal under an external field is investigated. We show that the magnetization reorientation may happen when the metastable state becomes unstable. With a comparison to the classical model, we suggest an explicit relation between the microscopic anisotropy param-

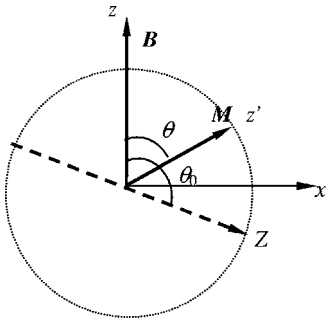

FIG. 1. Geometry of a monocrystal. The external magnetic field **B** is always along the z direction. The easy axis is presented by dashed line. When the field is absent, the angle between the magnetization **M** and z direction is θ_0. When **B** is applied, **M** turns to the z' direction. **M** changes in the xz plane and has two components $\langle S^z\rangle$ and $\langle S^x\rangle$.

eter K_2 in the Hamiltonian and the macroscopic one K_u, which can be measured experimentally. Then we study the magnetizing and magnetization reversal of a FM polycrystal. In both the monocrystal and polycrystal cases, the effect of temperature is emphasized.

II. THE MODEL AND METHOD

We first study the magnetization of a monocrystal in a field. The crystal structure is assumed to be simple cubic (s.c.). The geometry is shown in Fig. 1. $0 \le \theta_0 \le \pi$ and $-\pi \le \theta \le \pi$. Here θ is zero when **M** is along the z axis, and is positive (negative) when **M** is on the right (left) side of the z axis. The rotated frame where **M** is in the z' direction is hereafter called the primed frame, as in Ref. 8.

The Hamiltonian is

$$H = -\frac{1}{2}J\sum_{i,j}\mathbf{S}_i\cdot\mathbf{S}_j - K_2\sum_i (S_i^Z)^2 - \mathbf{B}\cdot\sum_i \mathbf{S}_i. \tag{1}$$

The three terms are the FM exchange, single-ion anisotropy energy, and Zeeman energy under an external magnetic field **B**, respectively. In this paper, we let the Boltzmann constant $k_B=1$ and Bohr magneton $\mu_B=1$ so that all the quantities, the exchange parameter J, anisotropy parameter K_2, temperature T, magnetic field **B**, and magnetization are measured in the unit of energies. We set $J=100$, $K_2=1$ and $S=1$. In Sec. IV C, we will discuss the effect of the variation of the spin quantum number S and anisotropy K_2.

The magnetization is the statistical average of the spin operator in the primed frame. $M=\langle S^{z\prime}\rangle$, as well as correlation function $\langle (S^{z\prime})^2\rangle$, is calculated by the retarded Green's function. Usually, in experiments, the magnetization component along the field direction is measured. Therefore, we mainly calculate $\langle S^z\rangle = M\cos\theta$, the magnetization component projected onto the field direction.

The FRM method was used by two different groups.[8,9] However, they gave different formulas for the energy spectrum. We tested both formulas to calculate **M** for a monodomain and found no visible difference in the numerical results. Hence, in this paper we use the formula in Ref. 8.

The energy spectrum of Hamiltonian Eq. (1) is

$$\epsilon_k = MJp_k + B\cos\theta + 2K_2MC_1 \times\left[\cos^2(\theta-\theta_0) - \frac{1}{2}\sin^2(\theta-\theta_0)\right], \tag{2}$$

where $p_k = 2(3-\cos k_x - \cos k_y - \cos k_z)$ and

$$C_1 = 1 - \frac{1}{2S^2}[S(S+1) - \langle (S^{z'})^2\rangle]. \tag{3}$$

III. RESULTS AND DISCUSSION OF A MONOCRYSTAL

For each monocrystal with θ_0 in the range $[0,\pi]$, $\langle S^z\rangle$ as a function of the field at several temperatures is computed. The field varies in such a way that it increases from zero to a value B_m, which is called magnetizing, and then decreases from B_m to $-B_m$, which is called magnetization reversal.

In FRM, we have an equation that determines the angle θ as follows:

$$\sin 2(\theta_0-\theta) = \frac{B}{K_2C_1M}\sin\theta. \tag{4}$$

This equation is from Ref. 8, but is written here in the form that agrees with the geometry of Fig. 1. It was obtained from the condition that $S^{z'} = \sum_i S_i^{z'}$ commutes with the Hamiltonian Eq. (1) since, in the primed frame, $S^{z\prime}$ is conserved. Here we show that this condition is equivalent to an energy minimum. The total energy E_T of the system is the statistical average of the Hamiltonian Eq. (1),

$$E_T = \langle H\rangle = -\frac{1}{2}J\left\langle\sum_{i,j}\mathbf{S}_i\cdot\mathbf{S}_j\right\rangle - K_2\left\langle\sum_i (S_i^Z)^2\right\rangle - \mathbf{B}\cdot\left\langle\sum_i \mathbf{S}_i\right\rangle.$$

The first term is isotropic. The third term is

$$-\mathbf{B}\cdot\left\langle\sum_i \mathrm{S}_i\right\rangle = -NB\langle S^z\rangle = -NBM\cos\theta.$$

Here N is the site number of the lattice. We have used the property that the lattice is of translation invariance. For the anisotropy term,

$$\langle (S_i^Z)^2\rangle = \sin^2(\theta_0-\theta)\langle (S_i^{x'})^2\rangle + \cos^2(\theta_0-\theta)\langle (S_i^{z'})^2\rangle + \frac{1}{2}\sin 2(\theta_0-\theta)\langle S_i^{x'}S_i^{z'} + S_i^{z'}S_i^{x'}\rangle,$$

where the last term is zero.[8,10] We can rewrite it as

$$\langle (S^Z)^2\rangle = \langle (S^{z'})^2\rangle - \sin^2(\theta_0-\theta)[\langle (S^{z'})^2\rangle - \langle (S^{x'})^2\rangle].$$

We neglect the terms independent of θ and let $E=E_T/N$ be the energy of each spin.

$$E = q\sin^2(\theta_0-\theta) - BM\cos\theta\square \tag{5}$$

where the coefficient of the first term is written by q. Taking $dE/d\theta=0$, one obtains a relationship between θ and θ_0, which was exactly the same as Eq. (4). Therefore, we think

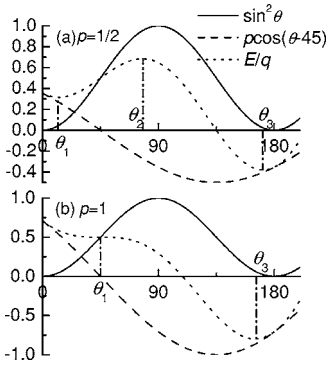

FIG. 2. The solid, dashed and dotted lines are $\sin^2\theta$, $-p\cos(\theta-45)$ and E/q, respectively. (a) $p=1/2$. (b) $p=1$.

that the energy of the state reaches the minimum at θ, satisfying Eq. (4).

When the field varies, **M** rotates subject to the field. Now we show, by analyzing Eq. (5), that the **M** reorientation of the crystallites happens when the field reaches a certain value and the metastable state becomes unstable. Let $p=BM/q$. We consider the case of $T=0$. At zero temperature, the magnitude of **M** as well as C_1 does not change during the **M** rotation. The energy is written as $E/q=\sin^2(\theta_0-\theta)-p\cos\theta$. We look at an example of $\theta_0=135°$. In Figs. 2(a) and 2(b), after the abscissa is translated by θ_0, $\sin^2\theta$, $-p\cos(\theta-45)$ and E/q are plotted in the cases of $p=1/2$ and 1, respectively. $\sin^2\theta$ is independent of p. When $p=0$, the field is absent. There are two energy minima at $\theta=0°$ and 180°, and one maximum between them. We let the spin be at the position of 0°. When $p=1/2$, the energy minimum is at θ_1 in Fig. 2(a). Although the minimum at θ_3 is lower, the maximum at θ_2 still exists. Therefore, when p increases from 0 to 1/2, the magnetization rotates continuously from 0° to θ_1.When this occurs, the maximum lowers. When p reaches 1, the maximum disappears and θ_1 becomes an unstable state, see Fig. 2(b). The magnetization goes to position θ_3 instantly. This is the so-called "reorientation."

Now the change of **M** can be either a continuous rotation or reorientation. Figures 3(a) and 3(b) show the trajectory of **M** in the case of $\theta_0=\pi/4$ as an example of $\theta_0<\pi/2$ at $T=10$. At the beginning, **M** is at position "A." As the field B increases, starting from zero to 3, **M** rotates toward the field direction, going from point "A" to "B" as in Fig. 3(a). There is no abrupt reorientation of **M**. As B decreases from 3 to −3, the magnetization trajectory is plotted in Fig. 3(b). With B decreasing, **M** turns away from the field direction. As $B=0$, it goes back to point "A." When B increases from zero in the opposite direction, **M** turns from point "A" to "C." In this region, $\langle S^z\rangle$ is positive. A leap from point "C" to point "D" occurs to make $\langle S^z\rangle$negative, and then **M** continues to turn to point "E."

Hereafter, when $\langle S^z\rangle$ and B have the same sign, we say that $\langle S^z\rangle$ is parallel to the field while, if they have opposite signs, we say that $\langle S^z\rangle$ is antiparallel to the field.

In the case of $\pi/2<\theta_0<\pi$, we need not draw the trajectory explicitly. The symmetry of the system helps us understand the trajectory from Fig. 3(b). For example, in the case of $\theta_0=3\pi/4$, we image that the magnetic field points down in Fig. 3(b) while the initial position of **M** remains unchanged. Then, with the field increasing from 0 to 3, **M** changes in the order of ACDE. The course of the magnetization change as the field decreases from 3 to −3 can also be easily analyzed.

We discuss the cases of $\theta_0<\pi/2$ and of $\theta_0>\pi/2$ separately because, in the course of B increasing from 0 to 3, reorientation occurs in the latter case while it does not occur in the former case. Figure 4(a) below also shows this difference.

Figure 3(c) and 3(d) shows the trajectory of **M** at $T=260$, a temperature close to the Curie point T_C. It is seen that at higher temperature, the magnitude of **M** varies with the field. As **M** turns closer to the field direction, its magnitude becomes larger.

The field causing the reorientation is called the critical field B_C. Figure 4(a) plots B_C versus θ_0 curves at $T=10$ by solid lines. When the field reaches $B_{C,\min}$, the magnetization with $\theta_0=3\pi/4$ can start to reorient. Therefore, $B_{C,\min}$ is the minimum values of the field causing **M** reorientation. The largest critical field is $2B_{C,\min}$ when θ_0 is equal to $\pi/2$.

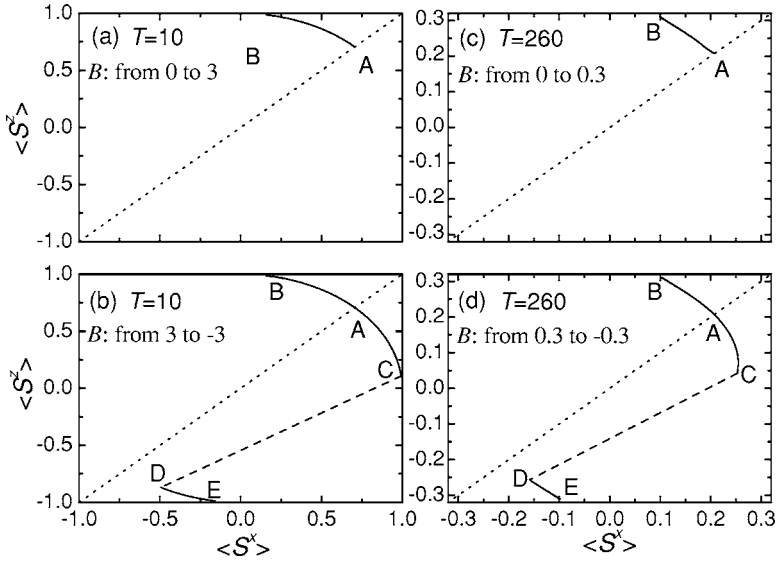

FIG. 3. Trajectories of **M** subject to the field in the case of $\theta_0=\pi/4$. (a) and (b) $T=10$. (c) and (d) $T=260$. The dotted lines show the easy axis. The solid lines show rotation and the dashed lines represent reorientation.

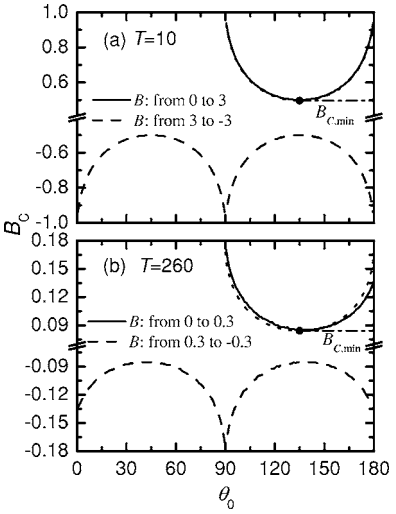

FIG. 4. The solid and dashed lines: B_C as a function of θ_0 determined by Eq. (4) at temperature (a) $T=10$ and (b) $T=260$. The dotted lines are drawn from Eq. (6).

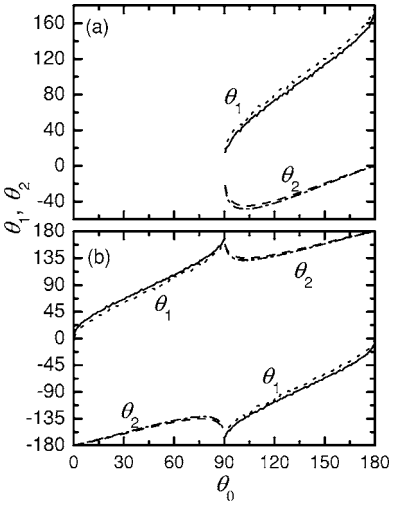

FIG. 5. The angles between **M** and **B** just before and after reorientation as a function of θ_0. The solid and dashed lines: B is from 0 to 3 in (a) and is from 3 to −3 in (b) at $T=10$. The dotted and dash-dotted lines: B is from 0 to 0.3 in (a) and is from 0.3 to −0.3 in (b) at $T=260$. When $\theta_0<\pi/2$, no reorientation happens in the magnetizing process. Therefore, there is no curve on the left of (a).

Let us make a comparison to the classical model. According to the classical model,[15] the relationship between B_C and θ_0 is determined by the equation

$$\sin 2\theta_0 = \frac{1}{p_C^2}\left(\frac{4-p_C^2}{3}\right)^{3/2},$$

where $p_C=B_C M/K_u$. This equation applies when the magnitude of **M** does not change during the rotation. Imitating this equation, we put down

$$\sin 2\theta_0 = \frac{B_{C,\min}^2}{B_C^2}\left(\frac{4-B_C^2/B_{C,\min}^2}{3}\right)^{3/2} \tag{6}$$

to indicate a supposed case in which the magnitude of **M** does not vary during the rotation. That is to say, **M** rotates like a classical magnetization, although its magnitude varies with temperature. The curve calculated by Eq. (6) is plotted in Fig. 4(a) as a dotted line. By the MBGFM, however, the magnitude of **M** varies during rotation. In Fig. 4(a), the solid and the dotted lines are nearly indistinguishable. This is the case of very low temperature where the magnetization is nearly saturated, and the difference in the magnetization change between the classical model and quantum model is trivial.

Figure 4(b) plots the curves of B_C versus θ_0 at a temperature of $T=260$. We also label the position of $B_{C,\min}$, and plot the curve according to Eq. (6) by dotted line. The solid line becomes asymmetric and deviates from the dotted line. This reflects the fact that, at higher temperature, the magnitude of **M** is more easily affected by the external field.

The quantity $B_{C,\min}(T)$ varies with temperature, and its temperature dependence is plotted in Fig. 9 below. It is, in fact, the coercivity of a monocrystal with $\theta_0=\pi/4$ at temperature T.

The angles just before and after the reorientation are denoted as θ_1 and θ_2, respectively. They are related to θ_0. In Fig. 5, θ_1 and θ_2 versus θ_0 curves are plotted at a temperature $T=10$ and 260, respectively. In the following discussion, the numbers (numbers in parenthesis) are for the case of $T=10$ (260). Figure 5(a) shows the case where B increases from zero to 3 (0.3). When $\theta_0<\pi/2$, there is no reorientation. Therefore, there is no curve on the left of Fig. 5(a). When $\theta_0>\pi/2$, reorientation occurs. The angle θ_1 ranges from some 15° (17°) to 171° (175°), and θ_2 ranges from zero to −45° (−49°). When $\theta_0<132°$ (127°), $\theta_1<\pi/2$, and when $\theta_0>132°$ (127°), $\theta_1>\pi/2$, which mean that $\langle S^z\rangle$ is parallel and antiparallel to the field direction before reorientation, respectively.

Figure 5(b) shows the case when B decreases from 3 (0.3) to −3 (−0.3). In the range of 48° (53°)$<\theta_0<$132° (127°), $\langle S^z\rangle$ is parallel to the field before reorientation. Outside of this range, $\langle S^z\rangle$ is antiparallel to the field before reorientation.

In all of the cases, after reorientation, $\langle S^z\rangle$ is always parallel to the field direction, and the angle between **M** and **B** is within $\pi/3$.

Figure 5 shows that the reorientation occurs more easily at higher temperatures than at lower temperatures, reflecting the fact that when the magnetization is smaller, the magnetization will be more easily forced to change.

We denote the $\langle S^z\rangle$ value just before and after reorientation as $\langle S_1^z\rangle$ and $\langle S_2^z\rangle$, respectively. Figure 6 plots the curves of $\langle S_1^z\rangle$ and $\langle S_2^z\rangle$ versus θ_0. Figure 6(a) shows the case of magnetization at a temperature of $T=10$. If $\langle S_1^z\rangle$ is antiparallel to the field, the reorientation makes $\langle S_2^z\rangle$ parallel to the field. If both $\langle S_1^z\rangle$ and $\langle S_2^z\rangle$ are parallel to the field, the latter is usually larger than the former. In most cases, the difference of $\langle S_1^z\rangle$ and $\langle S_2^z\rangle$ is enlarged as θ_0 rises. However, near $\theta_0=\pi/2$, the reorientation makes $\langle S_2^z\rangle$ smaller than $\langle S_1^z\rangle$. This is called abnormal reorientation. For example, at $\theta_0=93°$, the reorientation occurs when $B=0.84$. Before and after the reorientation **M** is (0.38,0,0.92) and (−0.57,0,0.82), respec-

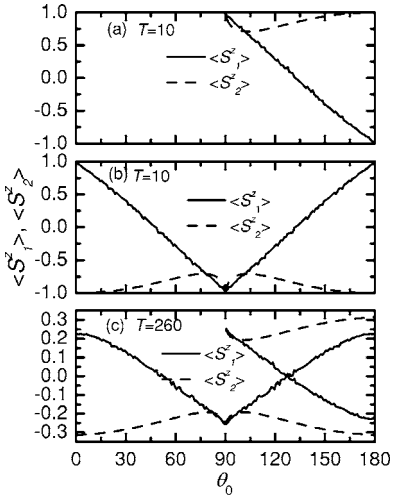

FIG. 6. $\langle S^z\rangle$ value just before and after **M** reorientation as a function of θ_0 when B varies. (a) B is from 0 to 3 at $T=10$. (b) B is from 3 to −3 at $T=10$. (c) B is from 0 to 0.3 and is from 0.3 to −0.3 at $T=260$.

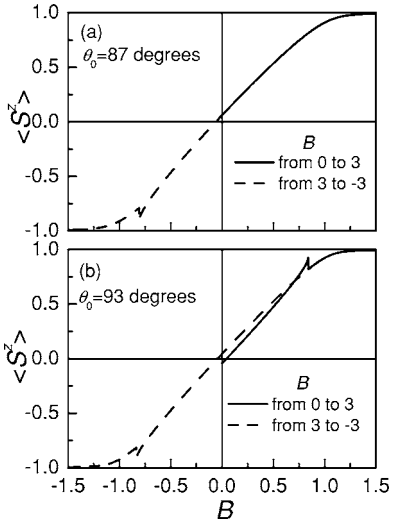

FIG. 7. Magnetizing and magnetization reversal curves of a monocrystal at $T=10$ with (a) $\theta_0=87°$ and (b) $\theta_0=93°$. The field value at which the tip appears is B_C. In the first quadrant of (a), the two curves are identical.

tively, while the magnitude of **M** remains unchanged. This means that, after reorientation, **M** is away from the field direction. In spite of this, **M** is sufficiently close to the easy axis that the drop of the anisotropy energy is more than the increment of Zeeman energy. As a result, the total energy is lower than that before reorientation.

Figure 6(b) shows $\langle S^z_1\rangle$ and $\langle S^z_2\rangle$ when B decreases. In both Figs. 6(a) and 6(b), $\langle S^z_1\rangle$ varies with θ_0 linearly. This is because, at low temperatures, the magnitude of **M** remains unchanged during rotation. Figure 6(c) shows the results at $T=260$. Curves of $\langle S^z_1\rangle$ versus θ_0 deviate from a straight line as, at this temperature, the magnitude of **M** is changed by the field. When θ_0 is around 0 or π, the change is the largest, in accordance with Fig. 4.

We calculated the magnetizing and magnetization reversal curves for various θ_0 at $T=10$ and 260, respectively (not shown). For most cases of θ_0, the curves at $T=10$ were almost exactly the same as those of the classical model.[1,15,16] At $T=260$ the curves showed that the magnitude of the **M** varied during rotation. A remarkable feature is that when θ_0 is around $\pi/2$, there were small tips on the curves which resulted from the abnormal reorientation. Figure 7 shows examples. As has been discussed above, around $\theta_0=\pi/2$, the abnormal reorientation causes $\langle S^z_2\rangle$ to be smaller than $\langle S^z_1\rangle$. Therefore, $\langle S^z\rangle$ drops as the field reaches B_C, which results in the tip on the curve. We believe that the tips can be detected in experiments.

Now let us discuss the anisotropy coefficient. The relation between the microscopic anisotropy K_2 and the macroscopic one, K_u, has been carefully studied in a number of papers.[17,18] Our goal is to put down a formula between the two quantities by comparing the present model to the classical one.

In the classical model, the magnetic crystalline anisotropy energy[1,15,16] is written as

$$E_K = K_u \sin^2(\theta_0 - \theta), \tag{7}$$

where K_u is the anisotropy coefficient, which can be measured experimentally. When a magnetic field is applied in the geometry of Fig. 1, the equation that determines the angle θ is, under the condition of an energy minimum,

$$\sin 2(\theta_0 - \theta) = \frac{MB}{K_u} \sin\theta. \tag{8}$$

By inspection of the right-hand side of Eqs. (4) and (8), one sees that M is in the denominator in the former and in the numerator in the latter. We think that this is an important difference between the classical and quantum models. From these two equations, the connection between K_2 and K_u is established as follows:

$$K_u(T) = K_2 C_1(T) M^2(T). \tag{9}$$

The anisotropy coefficient K_u is temperature dependent[19–21] and its variation with temperature was believed to be more rapid than the magnetization M.[19] Equation (9) shows that $K_u(T)$ depends on the square of the magnetization $C_1(T)M^2(T)$. According to RPA, as T approaches the Curie point T_C, the magnetization of an FM system goes to zero in the way of $M \propto (T-T_C)^{1/2}$. The temperature dependence of C_1 is embodied in Eq. (3). The correlation $\langle (S^{z\prime})^2\rangle$ of a monocrystal is a nearly linear function of temperature between zero and the Curie point, which is quite similar to the two-dimensional case.[4,5,22] We therefore do not plot the curve here. Based on this fact, we can approximate the correlation in the following way.

$$\langle (S^{z\prime})^2\rangle = \frac{2S-1}{2S}\left(1 - \frac{T}{3T_C}\right), \quad 0 \le T \le T_C. \tag{10}$$

Therefore, when $T \to T_C$,

$$K_u \propto (3T_C - T)(T - T_C) \propto T - T_C. \quad (11)$$

$K_u(T)$ goes to zero linearly with T. In Refs. 5 and 7, the free energy was written and included a term equivalent to Eq. (7), where K_u was denoted as $K_2(T)$ and was called the effective anisotropy coefficient. $K_2(T)$ was calculated under RPA and it, indeed, approached zero linearly with T.

With the form of Eq. (9) we can calculate K_u easily, while in Refs. 5 and 7 one had to apply a small field perpendicular to the easy axis to calculate K_u. The quantity $C_1(T)M^2(T)/C_1(0)M^2(0)$ as a function of temperature is calculated. It is not shown here because it is qualitatively the same as $K_2(T)/K_2$ calculated in Refs. 4, 5, and 7. We notice that its behavior is similar to measured K_u of some elements, such as Co,[19,20,23] Tb, and Dy[24] as long as the temperature was not close to transition point.

Besides the dependence of $M^2(T)$, the correctness of Eq. (9) is also related to the quantity C_1, which came from the decoupling procedure of the higher order Green's function $\langle\langle S^z S^+ + S^+ S^z; S^-\rangle\rangle$. The expression of Eq. (3) was from Anderson-Callen's decoupling.[25] It was shown by a quantum Monte Carlo calculation[26] that when the ratio of K_2/J was within some a few percents, the decoupling was good in almost the whole temperature range below the Curie point, and when K_2/J was larger, the decoupling was good only in low temperatures (see Fig. 1 of Ref. 12).

Please note that Eq. (10) is only suggested as a simplified form. In this paper, we always calculate the correlation function $\langle (S^{z\prime})^2\rangle$ by means of MBGFM.

IV. RESULTS AND DISCUSSION OF A POLYCRYSTAL

Having studied monocrystal in details, we now investigate a polycrystal, in which the easy axes of monocrystals are distributed uniformly over the full 4π solid angles. The magnetization of a monocrystal was denoted as **M**, and its projection to the field direction was $\langle S^z\rangle = M\cos\theta$. The magnetization component along the field direction of the polycrystal, denoted as M_p, is averaged $\langle S^z\rangle$ over equally weighted monocrystals. No effects due to noncollinear magnetizations at the crystal boundaries are considered, hence the magnetic reversal via domain wall motion is not considered. In the following, we will discuss the magnetizing process and corresponding susceptibility, the magnetization reversal process, and the remanence and the coercivity of a polycrystal.

A. Magnetizing curve

Figures 8(a) and 8(b) show a magnetizing curve and the corresponding susceptibility M_p/B versus B at $T=10$ and 200.

Let us first consider the solid lines in Figs. 8(a) and 8(b). The curves can be divided into three parts: that from the origin to point "A," that from point "A" to point "B," and that beyond point "B," which are called region I, II, and III, respectively. They correspond to a reversible rotation before reorientation, irreversible reorientation, and reversible rotation after reorientation of the magnetization, respectively.

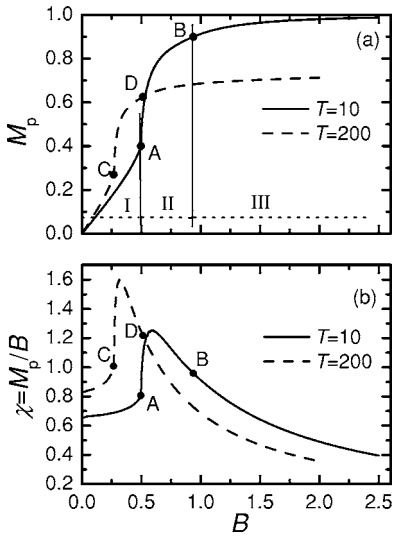

FIG. 8. (a) M_p and (b) M_p/B vs B of a FM polycrystal at $T=10$ and 200. In (a), the three regions of the solid are marked.

The field values at points "A" and "B" are $B_A = B_{C,\min}$ and $B_B = 2B_{C,\min}$, where $B_{C,\min}$ is the parameter in Eq. (6).

The three regions of the dashed lines in Fig. 8 are distinguished by letters "C" and "D," and the analysis of them is similar to the case of solid lines. In the following, we mainly discuss the solid lines, mentioning the dashed lines as a comparison where necessary.

In region I, when the field decreases, the magnetization goes back to the origin. M_p is almost linearly proportional to B. Hence, the susceptibility in this region is comparatively flat, as shown in Fig. 8(b).

Let us now discuss the differential susceptibility $\chi_d = (dM_P/dB)$ of a polycrystal. If we neglect the dependence of M and C_1 on θ, the differential susceptibility of a monocrystal χ_{dm} can be derived with the help of Eq. (4),

$$\chi_{dm} = \left(\frac{d\langle S^z\rangle}{dB}\right) = \frac{M\sin^2\theta}{2K_2C_1M\cos(\theta_0-\theta) - B\cos\theta}.$$

At each B, θ is determined in terms of B and θ_0 by Eq. (4). Then, taking the average of χ_{dm} with respect to θ_0, one obtains χ_d. However, because θ is dependent on θ_0, the average is difficult to calculate. The qualitative behavior of χ_d can be analyzed based on the magnetizing curves [see examples in Fig. 8(a)]. As a simple case, the initial differential susceptibility χ_i can be obtained. When the field is weak, the magnetization of a monocrystal rotates by a small angle. That is to say, $\theta_0 - \theta$ is small. The initial differential susceptibility of a monocrystal is

$$\chi_{im} = (\chi_{dm})_{B\to 0} = \frac{1}{2K_2C_1}\sin^2\theta_0.$$

The angular average of χ_{im} gives the value of χ_i of a polycrystal as

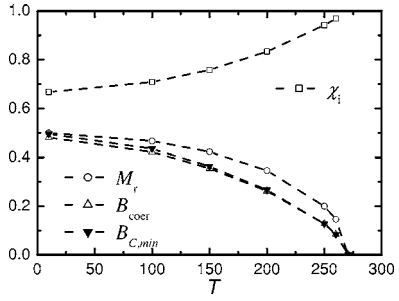

FIG. 9. The initial susceptibility χ_i, the remanence, and coercivity of a polycrystal as functions of temperature. The solid triangles are the coercivity of a monocrystal with $\theta_0=\pi/4$. They are plotted here to compare with B_{coer}. The dashed lines are to guide the eyes.

$$\chi_i = \frac{1}{3K_2C_1}. \tag{12}$$

As $B\to 0$, χ_i is the same as the initial susceptibility $(M_P/B)_{B\to 0}$. For instance, at $T=10$, $\langle(S^{z\prime})^2\rangle=1$, hence $\chi_i=0.67$; at $T=200$, $\langle(S^{z\prime})^2\rangle=0.83$, and, hence, $\chi_i=0.83$. They are in agreement with the results in Fig. 8(b).

Although the magnetization does not explicitly appear in Eq. (12), χ_i increases when the magnetization decreases. This is because when $M=\langle S^{z\prime}\rangle$ is smaller, $\langle(S^{z\prime})^2\rangle$ is also smaller, resulting in a smaller C_1. Figure 9 shows that χ_i increases with temperature. However, χ_i calculated in Fig. 9 is up to $T=260$, which is below the Curie point $T_C=271$. This is because Eq. (12) does not apply at $T=T_C$. At T_C, M is very small and the anisotropy energy is proportional to M^2 so that it is negligible compared to the Zeeman energy, which results in a divergent χ_i.

Here we should again make a comparison with the classical model. In the classical model, it is calculated that $\chi_i=M^2/3K_u$,[15] which is proportional to the square of the magnetization. The difference between the expression of the classical model and the quantum model is attributed to the difference between K_2 and K_u.

Region II between points "A" and "B" in the magnetizing curve is mainly due to the irreversible reorientation of magnetization. The field strength is between $B_{C,\min}$ and $2B_{C,\min}$, and the reorientation occurs within this region, as can be seen in Fig. 4. Because of the reorientation, M_p rises rapidly. The susceptibility in this region is the highest among the three regions [see Fig. 8(b)].

We have seen from Fig. 4 that, at higher temperatures, the irreversible reorientation occurs more easily. As a result, the susceptibility should rise with temperature. It is seen in Fig. 8(b) that, in region II, a higher temperature leads to a larger susceptibility.

Region III again reflects the reversible rotation of magnetization. In this region, the field B is above $2B_{C,\min}$, and the irreversible reorientation of the magnetizations of all monocrystals has been completed. As B increases further, they turn closer to the field direction, which is reversible, (see, for example, between points "A" and "B" or from "D" to "E" in Fig. 3). In this region, the susceptibility decreases with field strength and a smaller magnetization contributes to a smaller susceptibility [see Fig. 8(b)].

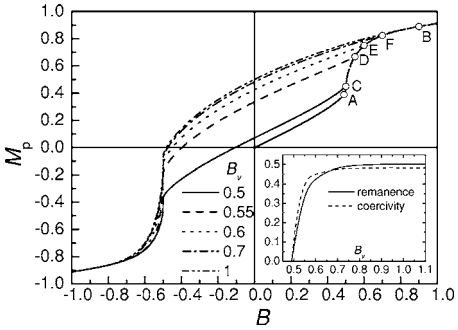

FIG. 10. Magnetizing and magnetization reversal curves at $T=10$. The inset: remanence and coercivity as functions of B_v at this temperature.

B. Magnetization reversal

Now we study the magnetization reversal. We first magnetize the polycrystal, i.e., raise the field from zero to a value B_v. Then we lower the field to zero and raise it in the opposite direction. Figure 10 shows the results of $B_A=B_{C,\min}$, $B_C=0.5$, $B_D=0.55$, $B_E=0.6$, $B_F=0.7$, and $B_B=2B_{C,\min}$ at $T=10$.

When B_v is less than B_A, the magnetization reversal curve is identical to the magnetizing one because, in this region, all the monocrystalline magnetizations rotate reversibly. When B_v is larger than B_A, a hysteresis loop, as well as the remanence M_r and coercivity B_{coer}, appear. M_r is the M_p value at $B=0$ on the magnetization reversal curve, and B_{coer} is the field value at which the magnetization M_p reorients from antiparallel to parallel to the field direction. They increase with B_v. When B_v is larger than B_B, the magnetization reversal curve is the same as when $B_v=B_B$. As $B_v\geq 2B_{C,\min}$, the loop does not change any more and its M_r and B_{coer} reach a maxima. The inset of Fig. 10 shows their dependence on B_v. Both increase with B_v rapidly, and quickly approach the maxima. In the following, we merely discuss the maximum M_r and B_{coer}.

Our calculation shows that, at any temperature, the remanence is $M_r(T)=M(T)/2$, where $M(T)$ is the magnetization of a monocrystal without an applied field. $M_r(T)$ is also equal to the remanence of a monocrystal with $\theta_0=\pi/3$. The open circles in Fig. 9(b) show $M_r(T)$ as a function of temperature.

The dependence of the coercivity $B_{\text{coer}}(T)$ on temperature is plotted by open triangles in Fig. 9. The coercivity of a polycrystal is quite close to that of a monocrystal with $\theta_0=\pi/4$, which is actually $B_{C,\min}(T)$ shown in Fig. 9. That is to say, the ratio $B_{C,\min}(T)/B_{\text{coer}}(T)$ is quite close to 1. It is even closer to 1 when the temperature goes to the Curie point, as can be seen in Fig. 9. For instance, $B_{C,\min}(10)/B_{\text{coer}}(10)=1.025$ and $B_{C,\min}(260)/B_{\text{coer}}(260)=1.001$.

C. Effect of varying the anisotropy parameter and spin quantum number

Figure 11 shows examples of varying the anisotropy parameter K_2 and spin quantum number S.

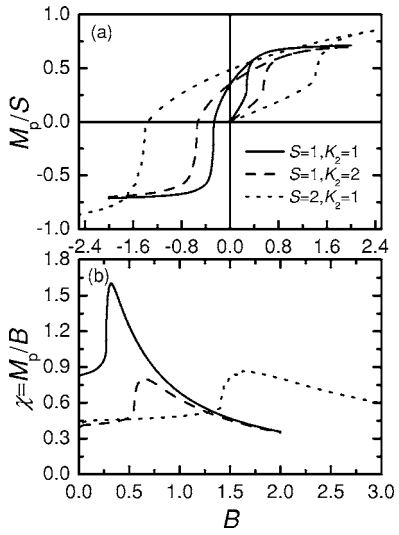

FIG. 11. (a) Magnetizing and magnetization reversal curves and (b) susceptibilities of polycrystals with different K_2 and S at $T=200$.

First, we discuss the effect of K_2 while S is fixed. From Fig. 11(a), it is concluded that the M_r of a polycrystal is independent of the K_2 value.

It is deduced from Eq. (4) that the coercivity is nearly proportional to K_2. Here we say "nearly" because, as K_2 varies, the magnetization M and, subsequently, C_1 will be changed slightly. In Fig. 11(a), the parameter K_2 of the solid line is half that of the dashed line. Hence, the coercivity of the former is about two times that of the latter.

The initial susceptibility χ_I is nearly the inverse of K_2 [see Eq. (12)]. Figure 11(b) shows that the value of χ_I of the solid line is about two times that of the dashed line. It is also seen that a polycrystal with a higher K_2 has a lower susceptibility under any field strength. As B is sufficiently large, the magnetization is very close to the field direction. In this case, the magnitude of M_p is almost the same as for different K_2 [see Fig. 11(a)]. Subsequently, under sufficiently large fields, the susceptibilities of the polycrystals with different K_2 are the same [see Fig. 11(b)].

Next we discuss the effect of varying S with a fixed K_2. A larger S means a larger magnetization; hence, M_r consequently becomes larger. From Eq. (4) the coercivity is approximately proportional to the magnetization, so that a larger S means a larger coercivity. The conclusion is that a larger S raises both remanence and coercivity, resulting in a larger loop area. The solid and dotted lines in Fig. 11(a) give the example.

From Eqs. (3) and (10) one sees that $2/3-1/3S \leq C_1(S) \leq 1-1/2S$, so that it is easily proven that for $S_1 < S_2$, $C_1(S_1) < C_1(S_2)$. From Eq. (12), χ_I can be seen to be the inverse of $C_1(S)$. Thus, a larger S causes a smaller χ_i. Figures 11(a) and 11(b) give an example of this. It is seen from Fig. 11(b) that, in region III, the susceptibility corresponding to the dotted line is greater than that represented by the solid line. This is because, in region III, the magnetizations of the monocrystals purely rotate after reorientation and, thus, a larger magnetization contributes to a larger susceptibility.

V. SUMMARY

In this paper, we have studied the magnetization of an FM polycrystal by MBGFM under RPA. The model is such that each monocrystal is uniaxial and is a monodomain. The directions of the easy axes of the monocrystals are uniformly distributed over a 4π solid angle. First, we calculate the magnetization $\mathbf{M}$ of a monocrystal under an external field for θ_0 in a range $[0, \pi]$. We show that the spin is in the state of minimum energy. The effect of temperature is studied. At a higher temperature, the field causing irreversible reorientation of $\mathbf{M}$ is lower. Furthermore, the magnitude of $\mathbf{M}$ will increase with an increase of B. At low temperatures, the behavior of the magnetization is closer to that of the classical model. The reorientation of $\mathbf{M}$ causes $\langle S^z \rangle$ to have an abrupt change. The abnormal reorientation makes $\langle S^z \rangle$ drop and, as a result, small tips appear on the hysteresis loops. By comparison with the classical model, we suggest that the temperature dependence of the experimentally measurable anisotropy coefficient K_u is expressed by Eq. (9). This equation also enables us to calculate K_u directly.

Having studied monocrystals in detail, the magnetizing process of a polycrystal is easily understood. The magnetizing curve can be divided into three regions, which reflect the magnetization's change in three field ranges: reversible rotation before reorientation, irreversible reorientation, and reversible rotation after reorientation. In the first two regions, the higher the temperature is, the higher the susceptibility, while in the third region, it is the opposite. The initial susceptibility χ_i can be calculated by Eq. (12).

The magnetization reversal curves are calculated. The results show that the remanence of a polycrystal is $M_r(T)=M(T)/2$, where $M(T)$ is the magnetization of a monocrystal at zero field. The coercivity of a polycrystal is very close to that of a monocrystal with $\theta_0=\pi/4$.

The effect of K_2 and S on the coercivity and χ_i can be analyzed by Eqs. (4) and (12). Qualitatively, a larger K_2 and S result in a larger coercivity and a smaller χ_i. The remanence is independent of the K_2 value.

This paper shows that it is possible to study FM polycrystals by means of the many-body theory.

*Email address: wanghuaiyu@mail.tsinghua.edu.cn

[1] E. C. Stoner and E. P. Wohlfarth, Philos. Trans. R. Soc. London, Ser. A **240**, 599 (1948).

[2] S. V. Tyablikov, *Methods in the Quantum Theory of Magnetism* (Plenum, New York, 1967).

[3] H. B. Callen, Phys. Rev. **130**, 890 (1963).

[4] P. Fröbrich, P. J. Jensen, and P. J. Kuntz, Eur. Phys. J. B **13**, 477 (2000).

[5] P. Fröbrich, P. J. Jensen, P. J. Kuntz, and A. Ecker, Eur. Phys. J. B **18**, 579 (2000).
[6] Huai-Yu Wang, Chong-Yu Wang, and En-Ge Wang, Phys. Rev. B **69**, 174431 (2004).
[7] Huai-Yu Wang, Zhen-Hong Dai, P. Fröbrich, P. J. Jensen, and P. J. Kuntz, Phys. Rev. B **70**, 134424 (2004).
[8] S. Schwieger, J. Kienert, and W. Nolting, Phys. Rev. B **71**, 024428 (2005).
[9] M. G. Pini, P. Politi, and R. L. Stamps, Phys. Rev. B **72**, 014454 (2005).
[10] Huai-Yu Wang, Bin Zhou, and Nian-Xian Chen, Commun. Theor. Phys. **43**, 753 (2005).
[11] Huai-Yu Wang, Yao Long, and Nian-Xian Chen, Commun. Theor. Phys. **45**(1), 175 (2006).
[12] Huai-Yu Wang, S. U. Jen, and Jing-Zhi Yu, Phys. Rev. B **73**, 094414 (2006).
[13] Huai-Yu Wang, Chen Huang, Meichun Qian, and En-Ge Wang, J. Appl. Phys. **95**, 7551 (2004).
[14] P. J. Jensen, K. H. Bennemann, D. K. Morr, and H. Dreyssé, Phys. Rev. B **73**, 144405 (2006).
[15] S. Chikazumi and S. H. Charap, *Physics of Magnetism* (Robert E. Krieger Publishing Company, Inc., Malabar, FL, 1984).
[16] D. Jiles, *Introduction to Magnetism and Magnetic Materials* (Chapman and Hall, New York, 1991).
[17] P. J. Jensen and K. H. Bennemann, Solid State Commun. **105**, 577 (1998).
[18] C. Timm and P. J. Jensen, Phys. Rev. B **62**, 5634 (2000).
[19] *Ferromagnetic Materials: A Handbook on the Properties of Magnetically Ordered Substance*, edited by E. P. Wohlfarth (North-Holland, Amsterdam, 1980), Vol. 1.
[20] R. M. Bozorth, *Ferromagnetism* (D. Van Nostrand, Inc., New York, 1951).
[21] B. Coqblin, *The Electronic Structure of Rare-Earth Metals and Alloys: The Magnetic Heavy Rare-Earths* (Academic, New York, 1977).
[22] P. Fröbrich and P. J. Kuntz, Eur. Phys. J. B **32**, 445 (2003).
[23] R. M. Bozorth, J. Appl. Phys. **8**, 575 (1937).
[24] J. J. Rhyne and A. E. Clark, J. Appl. Phys. **38**, 1379 (1967).
[25] F. B. Anderson and H. Callen, Phys. Rev. **136**, A1068 (1964).
[26] P. Henelius, P. Fröbrich, P. J. Kuntz, C. Timm, and P. J. Jensen, Phys. Rev. B **66**, 094407 (2002).